JOURNAL OF THEORETICAL AND APPLIED MECHANICS
3, **39**, 2001

ROLLING CONTACT PROBLEM – FATIGUE CRACK PROPAGATION IN A SURFACE LAYER

Mirosław Olzak
Paweł Pyrzanowski
Jacek Stupnicki

Institut of Aeronautics snd Applied Mechanics, Warsaw University of Technology
e-mail: jstup@meil.pw.edu.pl

The paper deals with the problem of development of fatigue cracks in a surface layer, which is at present one of the most actual issues of contact mechanics. The results obtained by the authors from experimental and numerical investigations of the factors, which exert an essential influence on the propagation process of a crack of the "squat" type in the wheel/rail contact zone are presented.
In the first part of the work, the results obtained using the Immersion Method of Holographic Interferometry from the investigation into the shapes of faces of the cracks detected in rail heads are presented. Furthermore the experimental investigations into crack faces interactions conducted on the samples made of 900A steel under complex loads obtained by means of the Grating Holographic Interferometry are presented as well.
In the second part of the paper, the results of numerical investigations into 3D cracks of the "squat" type are discussed, with a complex stress state in the contact zone, stresses due to rail bending, residual stresses as well as thermal stresses taken into account. The investigations of the effect of conditions of crack faces interaction on simulation results, which have been conducted using 2D models are presented as well. Eight different cases were considered, and the results having the form of Stress Intensity Factor K_{II} courses versus the load position relative to the crack are presented.
In the last part of the work the results of numerical simulations of rolling the wheel over the raceway with an oblique crack are presented. The conditions of crack faces interaction used in simulations were determined, basing on the experimental investigations.

Key words: contact mechanics, fatigue and fracture, computational mechanics, holographic interferometry

1. Introduction

The analytical model of contact formulated by Hertz in 1882 can be considered as a milestone in mechanics of contact (Hertz, 1882). For the first time, basing on his observations and results of interferometry measurements Hertz formulated a hypothesis of elliptical shape of the contact area. He also put forward a suggestion that for the sake of simplicity one could assume that the body in contact could be considered as an elastic half-space subject to a local load distributed over an elliptical area. That simplification made it possible to assume that complex concentrated contact stresses and the general stress state due to object shape, total load and way of its support, respectively, might be superimposed.

The fundamental hypotheses of Hertz put also forward the assumptions that surface curvatures of the bodies in contact are continuous; bodies are elastic and homogeneous; deformations are small and there are no tangential reactions, therefore no friction appears. Later, all these assumptions were rejected in turn; namely, non-elastic bodies were considered in terms of rigid-plastic or elastic-plastic models, or linear visco-elastic ones. Close attention was paid to the tangential reactions, assuming at firsts the developed friction over the whole contact area. In the 1950s the works of McEvan, Poritsky, Johnson and Deresiewicz were devoted to determination of the contact sub-areas, in which microslips did not appear (stick zones, in which friction was not developed) an the sub-areas of microslips, in which the developed friction appeared.

The beginning of the 1960s brought about some successes in investigating of the lubricant effect on the contact stresses. At the initial stage of investigations the attention was focused on measuring a thickness of a lubricating film. In 1935 Merit started the investigations into this problem by means of simulating the meshing conditions of two teeth using a two-roller machine (Merritt, 1938). Later on, the measurements of electric resistance and capacitance as well as permeability of the X-ray beam tangent to the contact area were used in determination of a lubricant film thickness.

The first attempts at experimental measurement of pressure distribution in a lubricating film made by Pepler in 1938 did not yield the expected results. The development of experimental techniques brought about the effects not earlier than in the 1960s, when manganine sensors were introduced having the form of a thin film deposited over a surface of the roller raceways (Kannel, 1965-66; Kannel et al., 1965). Application of those sensors for the first time allowed for proving that under the EHD lubricating conditions the pressure "peak" predicted by Grubin (1949) in a rear side of the contact area really

existed. That time also the photoelastic method was introduced into a measurement of pressure distribution in a lubricant film, while models made of glass allowed for application of high contact pressure (Stupnicki, 1971).

The interferometry method employed by Gohar and Cameron (1966) proved that the thickness of lubricating film was constant over a major part of the contact area, supporting once again the assumption of Grubin.

New possibilities offered by the development of computation techniques allowed for formulation in the 1960s and 1970s more and more advanced numerical models of the EHD lubrication, representing in a more accurate way the effect of lubricant on the contact phenomenon (Lisegang, 1969; Krzemiński-Freda, 1969).

At the end of the 20th century the attention was focused on local problems, i.e., the contact area that had been considered before as a small one as compared to the whole object became a domain, in which the processes considered took place in sub-regions, i.e. in very small parts of the contact zone.

The stress state due to contact loads, i.e. 3D compressive stresses, which are time-variable of high magnitude and large gradients, exerts a substantial influence on those processes. Even at rather small surface roughness, the local pressures may exceed many times the magnitudes resulting from the formulae of Hertz. The pressure concentrations of similar magnitudes arise on a perfectly smooth surface as well, when there exist surface braking cracks (Dubourg and Kalker, 1993; Pyrzanowski, 1997). An important factor affecting the material effort in the contact region consists in the presence of residual stresses of a complex distribution. In many cases the magnitudes of these stresses can vary within the range $-500 \div +250\,\mathrm{MPa}$ (Bijak-Żochowski and Marek, 1997; Świderski, 1992). The local problems of the contact area consist also in non-homogeneity of a material, defects of a structure and material defects in the form of non-metallic inclusions of higher or lower hardness as compared to the native material, which affect pressure concentrations. When analysing the material effort in the contact area one should take into account the wear processes taking place on a surface as well as the thermal processes due to energy dissipation.

The liquid covering the contact surfaces, which may penetrate voids or cracks plays also an important role in the process (Bover, 1988; Bogdański, 1999).

The present work is devoted to the most actual and important local problem of contact mechanics, i.e., to the fatigue crack propagation in a surface layer of the contact zone. That subject has both cognitive and applicability

aspects since the majority of machine elements operating under the contact stresses are damaged due to fatigue crack propagation. The authors focus their attention on the problem of fatigue crack propagation in rail raceways. Those cracks often called "squat" or "black spot", appeared in the 1980s in high-speed lines, where high components of the traction forces necessary for overcoming the resistance to motion are combined with the normal loads. In Poland cracks of that type appeared in the end of the 1990s in the tracks in which ten years earlier the rails of higher strength properties, resistant to abrasive wear had been used.

2. Types of cracks appearing in the contact area

Generally, the cracks appearing in the rolling contact area can be divided into the following two groups:

- Cracks initiated inside the bodies in contact
- Surface breaking cracks.

The first group of cracks comprises those initiating mainly due to structural defects and, from the viewpoint of tribology, are not so interesting. Therefore, the second group should be considered, i.e., the cracks initiating at the surface due to contact loads and propagating inside the bodies. Cracks of that type can be found in different structures; namely, toothed wheels of gears, rolling bearings elements, railway wheels and rails raceways, etc.

The first works devoted to the considered problem were published in the early thirties. In the 1960s mainly the cracks initiating in toothed wheels of gears and rolling bearings were investigated. As a result, some characteristic types of cracks, like "pitting" or "spalling" were distinguished. These types comprise spallings of the raceway. The term "pitting" denotes small defects, of the several dozen μm in size, looking like pinhole porosity. While the term "spalling" represents defects of bigger sizes, up to several mm in length and thickness of decimal parts of mm (Batista et al., 2000).

Recently, for economic reasons, close attention is paid to the problem of crack initiation and propagation in rail heads. The catalogues of rail defects ([1, 17] containing the information collected over many years of exploitation provide descriptions of the defects like "shelling" or "head checking". Both these defects arise in the areas adjacent to the rolling surface. The term "shelling" represents spallings initiated by longitudinal scratches propagating then in a form close to the cracks of "spalling" type, while "head checking" comprises

oblique cracks initiating in a lateral surface of the rail head and propagating perpendicularly inside. Both these defects arise usually in the outer rail of a rail arc, where besides the normal rolling contact the wheel flanges get into contact with the rails, and the normal loads are accompanied by substantial slips on the contact area.

Nowadays, fatigue cracks of the "squat" type attract most attention of the researchers. These cracks were detected in rails in Western Europe and Japan several years ago, while in Poland they have been observed in high-speed lines since the end of the 1990s. These cracks can serve as a good example of a local problem of contact mechanics and need explanation of grounds of fatigue cracks initiation and propagation under conditions of rolling contact. In many works propagation of a crack of this type was modelled, e.g., (Keer and Briant, 1983; Bover, 1988; Bogdański et al., 1996b, 1998), however, some problems still need attention and detailed explanation.

In the work (Deroche et al., 1993) presenting investigations into grounds of cracks of the "squat" type detected in rails along railway lines Paris-Starsbourg and Paris-Bordoux very interesting remarks can be found: "Early stages of squat observed in French network are aligned in a narrow strip, propagation occurs into the rails in the rolling direction".

In ferrite pearlite steels the crack initiated at the surface occurs in heavily deformed proeutectoid ferrite layers. In pearlite steels no single initiation has ever been observed. The top layer $(50 - 150\ \mu\text{m})$ of the running strip is hardened reaching the maximum strength of metal. Due to high tangential stresses the grains are heavily deformed and shifted opposite to the rolling direction.

"Squats" can be found in high-speed conventional lines but they are also found in tangent tracks, where the slopes require high traction forces to drive heavy trains.

The early stage of "squat" initiation is associated with the grain boundary void alignment. The "squat" will form when plastic deformation is complete.

In some cases there arises a white phase layer (about $150\,\mu$m thick and of 760 Vickers hardness) the "squat" initiates at the interface between the white phase and steel substrate. The vertical cracks observed in a white phase layer are independent of the oblique ones in the ferrite substrate. The "squats" are independent also of the white phase existence.

The commonly accepted form of crack of the "squat" type is presented in Fig. 1. In a plate cut off from a rail, two branches of a crack can be seen. The longer one with some branching follows the direction of rolling, while the shorter one takes the direction opposite to the load motion. The crack

propagating in the direction of motion often turns to a crack penetrating the whole rail.

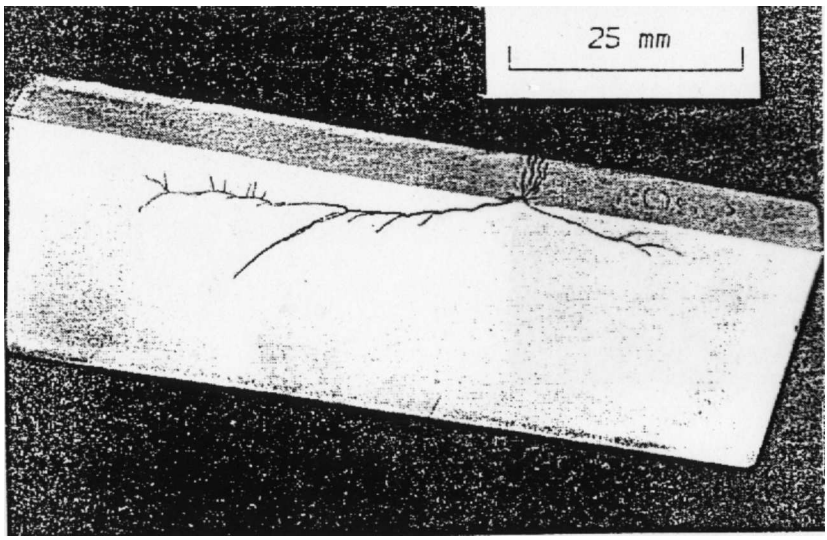

Fig. 1. Crack of the "squat" type

The cracks observed in rails of Polish Railways have a slightly different form. Fig. 2 shows a typical one. Also in this case the crack initiates on the rolling strip, its form, however, observed on the race way resembles a horseshoe, (it is, therefore, called the horseshoe crack) and reveals a very complex shape of the surface. Its shape will be described in the next section.

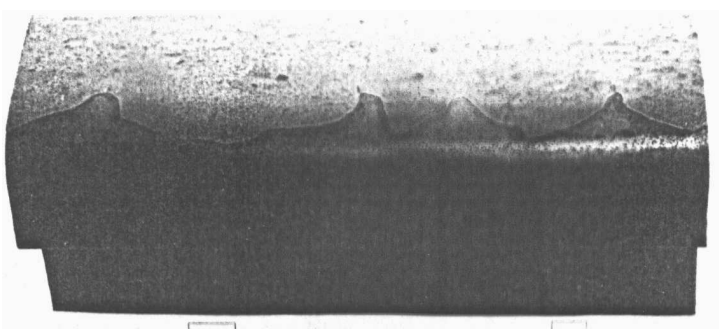

Fig. 2. Photo of a crack of the "squat" type appearing in rails in Poland

3. Macro and microscope investigations of cracks of the "squat" type

As mentioned above, fatigue cracks of the "squat" type appeared in the hardened raceways of rails in tracks laid by Polish Railways in the end of the eighties. Examination of their shapes and structures of faces proved that the examined cracks had many common features (Pyrzanowski and Mruk, 2000). Shapes of the crack surfaces were examined by means of the immersion method of holographic interferometry, as well as a profilograph. The visual observation allowed for determination of the crack arrest lines and crack boundaries at early stages of the crack development.

The authors found out that the crack of "squat" type initiated on a rolling strip in the wheel-rail contact area on the rail surface. Initially, the crack propagates in the direction making a relatively high angle with the surface (up to $70°$). On the surface the crack can be seen as a thin line, according to different authors making an angle of about $45°$ with the rail axis, or according to the results of our investigations, almost parallel to the axis. After reaching a length of about $2 \div 3$ mm the crack begins to turn assuming a characteristic shape in the course of propagation (see Fig. 3). Then, penetrating about $6 \div 7$ mm deep inside the rail head the crack propagates almost parallel with the rail head surface. Fig. 4 shows the contour lines of the crack face.

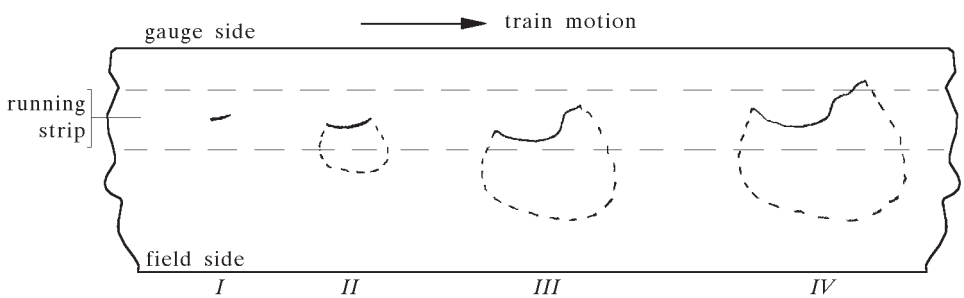

Fig. 3. Squat type crack in the four stages of growth

In Fig. 4 the arrows show the points of crack initiation, while the black lines represent consecutive positions of the arrest lines. Fig. 4a presents also the A ÷ D lines of 4 mm in length, along which the profiles of microaspherities shown in Fig. 5 were examined.

Fig. 6 shows the histograms of microaspherities measured along the lines A ÷ D.

Table 1 presents the values of roughness parameters R_a and R_{max}.

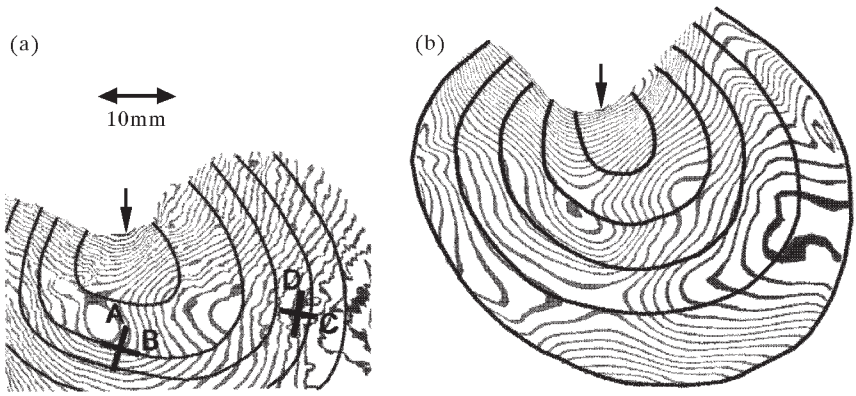

Fig. 4. Contour lines of two sample crack faces of the "squat" appearing in Polish rail tracks

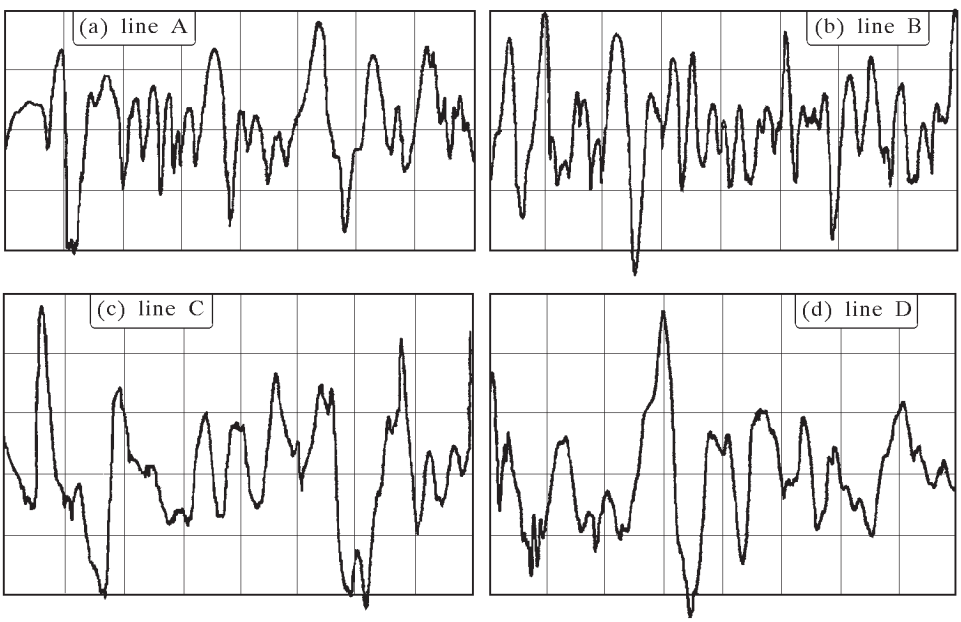

Fig. 5. Crack roughness distribution

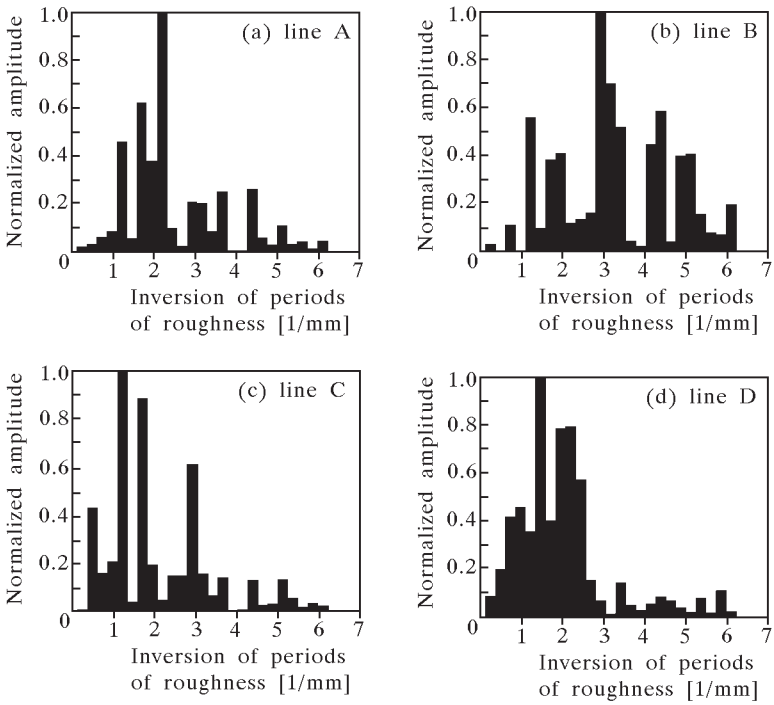

Fig. 6. Histograms of periods of crack roughness

Table 1. Parameters of roughness on the lines A ÷ D

Parameter	Line			
	A	B	C	D
R_a [μm]	5.68	6.12	7.29	7.03
R_{max} [μm]	38.20	43.18	54.74	52.36

The experimental investigation into roughness distribution serving as a source of input data for numerical simulation may also be helpful in understanding of the process of crack tip propagation by analysing the conditions of crack development.

4. Experimental investigation of crack faces interaction under normal and tangential loads

Many numerical simulations have been performed over the last few years,

which aimed at finding main factors affecting most strongly the propagation of fatigue cracks of the squat type. From the analysis of the results obtained the conclusion emerged that a more realistic representation of the crack faces interaction was strongly needed.

Therefore, the Grating Holographic Interferometry (GHI) has been employed, which allowed for determination of the relative displacements of crack faces in samples with the fatigue cracks produced before testing. Deformations in the crack-adjacent zone and the interaction between the crack face asperities have been determined, as well (Szpakowska, 2000; Pyrzanowski and Stupnicki, 2001).

4.1. The examined object

Samples made of 900A steel (used in production of railway rails) were examined. Samples of the shape shown in Fig. 7 containing a crack of $a \approx 20$ mm in length produced in tension were subject to the forces tangential P_t and normal P_n, respectively, to the crack plane. The forces were step-wise increased within the range from $P_0 \approx 0$ to $P_{max} = 10.5$ kN and the displacement distribution around the crack was registered at each step.

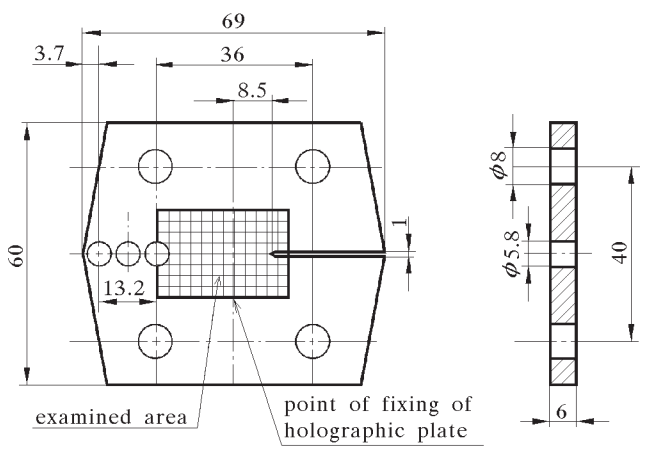

Fig. 7. Examined sample

In the course of investigations a step-wise increase of tangential and normal loads following the schemes presented in Fig. 9 was employed. Increments of the displacement vector components at sample surface points were registered as well.

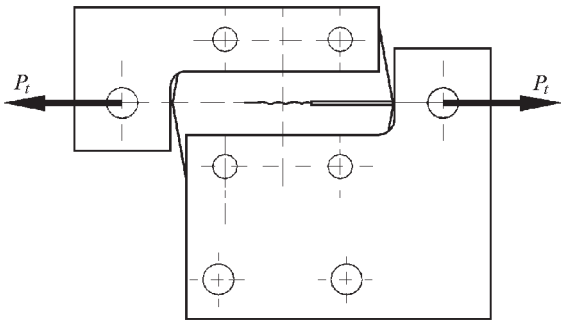

Fig. 8. Sample with the grips enabling the tangential load to be introduced

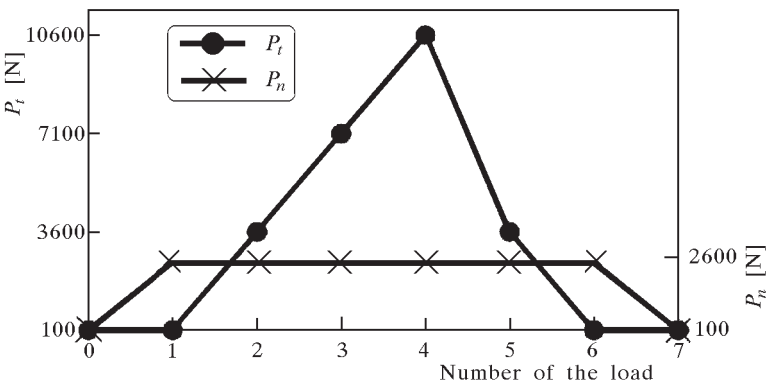

Fig. 9. Scheme of the step-wise increase of P_t and P_n loads

Fig. 10 presents a set of four interferograms reconstructed from a single holographic plate for a given step of load increasing.

Using two of the four interferograms the components of displacement vector were determined from Eqs (4.1) and (4.2), which were derived in (Szpakowska, 2000). The interferograms a) and d) presented in Fig. 10 were employed in the determination of v and w_1 components in the plane zy according to Eqs (4.1), while the interferograms (b) and (c) were used for the determination of components u and w_2 in the plane zx using Eq. (4.2). By comparing the values of the components w_1 and w_2 normal to the sample surface calculated from two different sets of interferograms one can check the measurement accuracy and verify the fringe order accepted

$$w_1 = \frac{\lambda}{2(1+\cos\theta)}(N_{1y} + N_{2y}) \qquad v = \frac{\lambda}{2\sin\theta}(N_{1y} - N_{2y}) \tag{4.1}$$

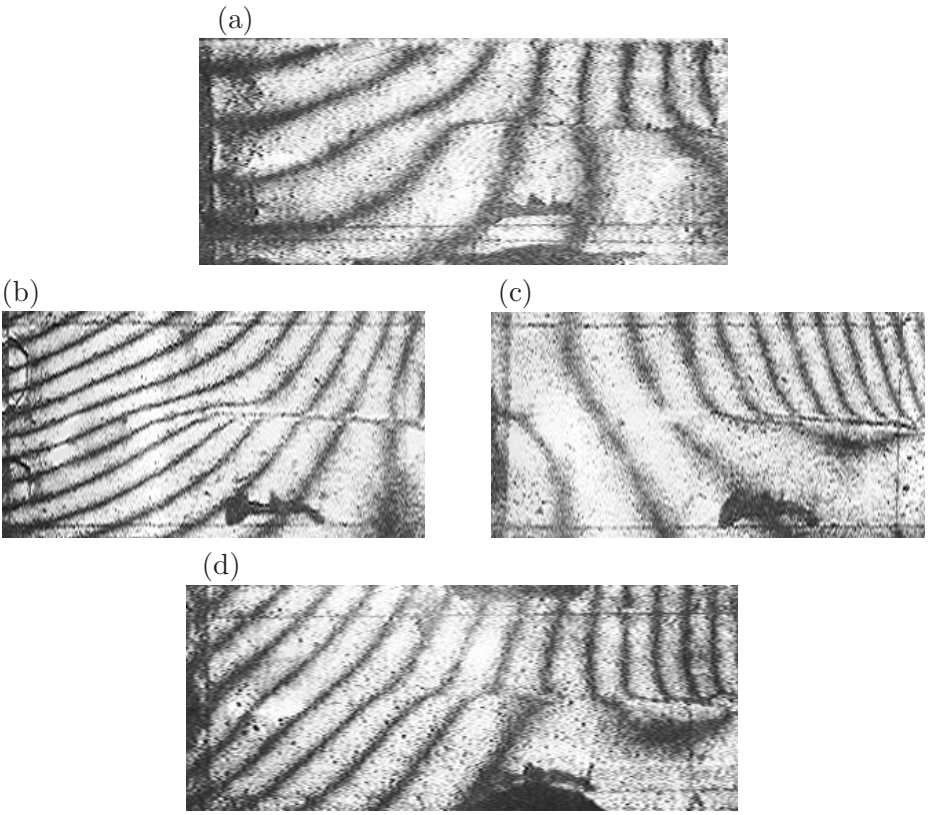

Fig. 10. Interferograms for the tangential load increase $\Delta P_t = 3500\,\mathrm{N}$, at $P_n = 2600\,\mathrm{N} = \mathrm{const}$; (a) image of N_{1y} fringes, (b) image of N_{2x} fringes, (c) image of N_{1x} fringes, (d) image of N_{2y} fringes

$$w_2 = \frac{\lambda}{2(1+\cos\theta)}(N_{1x} + N_{2x}) \qquad u = \frac{\lambda}{2\sin\theta}(N_{1x} - N_{2x}) \tag{4.2}$$

where N_{1y}, N_{2y} and N_{1x}, N_{2x} – fringe orders at the considered point on the interferograms (a), (b), (c) and (d), respectively.

The diagrams of components u, v, and w of the displacement vector in the cross-section located at a distance of 0.25 mm above the crack are presented in Fig. 11. for the tangential load increasing step equal to $\Delta P_t = 3500\mathrm{N}$, at $P_n = 2600\ \mathrm{N} = \mathrm{const}$.

4.2. The results obtained

Basing on the diagrams of the displacement vector at the points located along the lines parallel to the crack faces, which were determined for consecu-

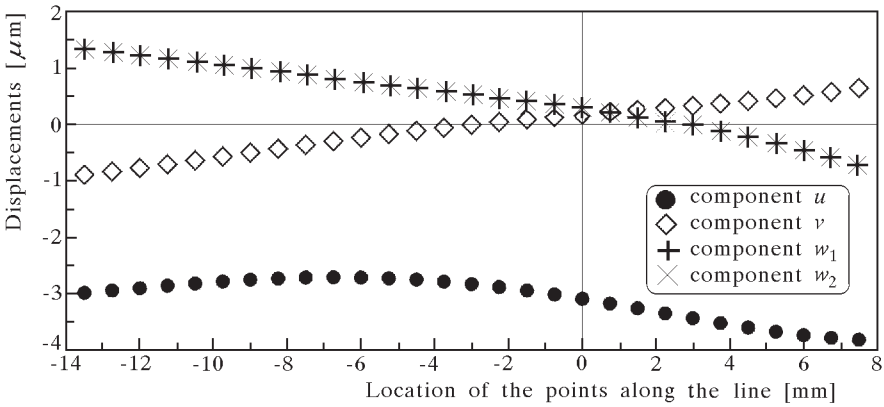

Fig. 11. Components u, v, w_1 and w_2 of the displacement vector at the points of sample surface located along the line at a distance of 0.25 mm from the crack

tive steps of the load increasing, descriptions of the processes of crack opening or closing and relative microslips of the crack faces were produced.

Resulting from the interferograms shown in Fig. 10. the distributions of microslips Δu_s and crack closing Δv_s, respectively, for a sample subject to shear at a constant magnitude of P_n, are presented in Fig. 12.

Fig. 13 presents a sum of the microslips Δu_s and crack dilatation Δv_s, for three consecutive steps of the load increasing. The same magnitudes of tangential force increments $\Delta P_t = 3300\,\mathrm{N}$ affected different displacement distributions and crack faces interactions.

The components of strain tensor in the layers adjacent to the crack faces were determined basing on numerical differentiation of the components u and v of displacement vector. The formulae for small deformations were employed

$$\varepsilon_{xx} = \frac{\partial u}{\partial x} \qquad \varepsilon_{yy} = \frac{\partial v}{\partial y} \qquad \varepsilon_{xy} = \frac{\partial u}{\partial y}\frac{\partial v}{\partial x} \tag{4.3}$$

Assuming that the material remained elastic, the components of stress tensor were found

$$\sigma_{xx} = \frac{E}{1-\nu^2}(\varepsilon_{xx} + \nu\varepsilon_{yy}) \qquad \tau_{xy} = \frac{E(1-\nu)}{2(1-\nu^2)}\varepsilon_{xy}$$
$$\sigma_{yy} = \frac{E}{1-\nu^2}(\varepsilon_{yy} + \nu\varepsilon_{xx}) \tag{4.4}$$

Fig. 14 shows the diagrams of the stress tensor component $\Delta\tau_{xyi}$, along the x axis at the third step of load increasing. The values of stress tensor

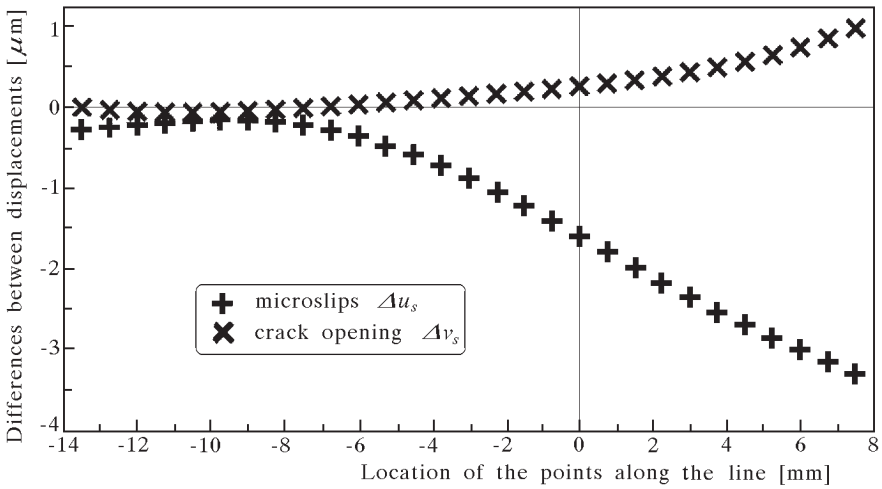

Fig. 12. Diagrams of differences between the displacements of the points located above and beneath the crack plane, respectively, which represent the crack opening Δv_s and microslips on the crack surface Δu_s

components were calculated as mean values of those determined in the cross-sections located at a distance of 1 mm above and beneath the crack plane, respectively.

Fig. 15 presents a sum of the stress tensor component $\Delta\tau_{xyi}$ at three consecutive steps of the load increasing.

Fig. 16 shows in a simplified form a section of a layer of sample containing the crack. The crack faces are separated from each other by a thin layer of wear product deposits. The space occupied by the wear products is bigger then the volume of material wear due to oxidation processes, dust, humidity and porosity of the layer. The increments of normal stress components $\Delta\sigma_{yyi}$ cause the layer thickness decrease Δv_{si} (Fig. 16b). The ratio of $\Delta\sigma_{yyi}$ to Δv_i at a given point on the crack faces is defined as the normal rigidity of the crack containing layer at the ith step of load increasing

$$K_{yyi} = \frac{\Delta\sigma_{yyi}}{\Delta v_{si}} \tag{4.5}$$

The increment of shear stress component $\Delta\tau_{xyi}$ affects the tangential displacement of the layer edges Δu_{si}.

The ratio between the increments of the tangential stress component $\Delta\tau_{xyi}$ and the mutual tangential displacements of the layer edges Δu_{si} (Fig. 16c) is

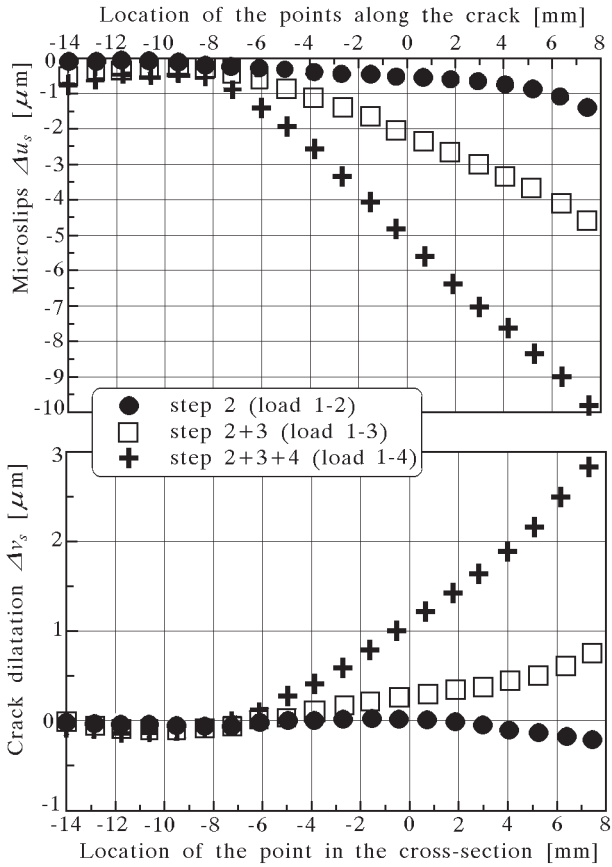

Fig. 13. The sum of the microslips Δu_s and crack dilatation Δv_s for three consecutive steps of the load increasing

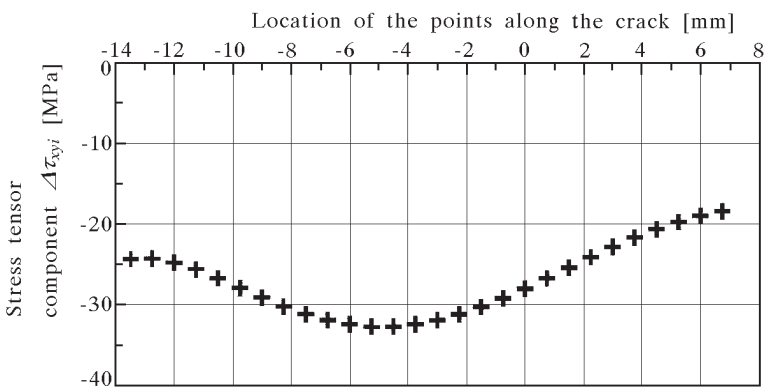

Fig. 14. Increments of the stress tensor component $\Delta\tau_{xyi}$ at the third step of load increasing

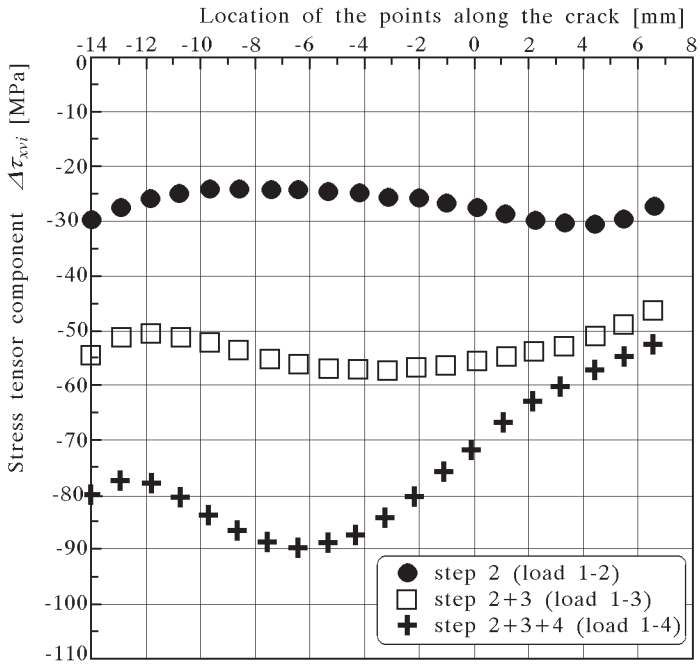

Fig. 15. The sum of the stress tensor component $\Delta\tau_{xyi}$ at three consecutive steps of the load increasing

defined as the tangential rigidity of the crack containing layer

$$K_{xyi} = \frac{\Delta\tau_{xyi}}{\Delta u_{si}} \tag{4.6}$$

It is worthwhile to note that the tangential displacements of the layer edges cause the crack dilatation, which manifests through the layer thickness increase Δv_{di} (Fig. 16c).

Basing on the distribution of increment of the shear stress $\Delta\tau_{xyi}$ along the crack shown in Fig. 14. and the corresponding increments of tangential displacements Δu_{si} (Fig. 13.) the tangential rigidity K_{xyi} was determined at a given step of load increasing.

The diagram of tangential rigidity K_{xyi} along the crack length at the third step of tangential load increasing at the constant normal load $P_n = 2600\,\mathrm{N}$ is shown in Fig. 17.

Calculations of K_{yyi} and K_{xyi} at consecutive steps of the load increasing allow for determination of the courses of rigidities versus the load level, which are useful in numerical simulations of crack propagation.

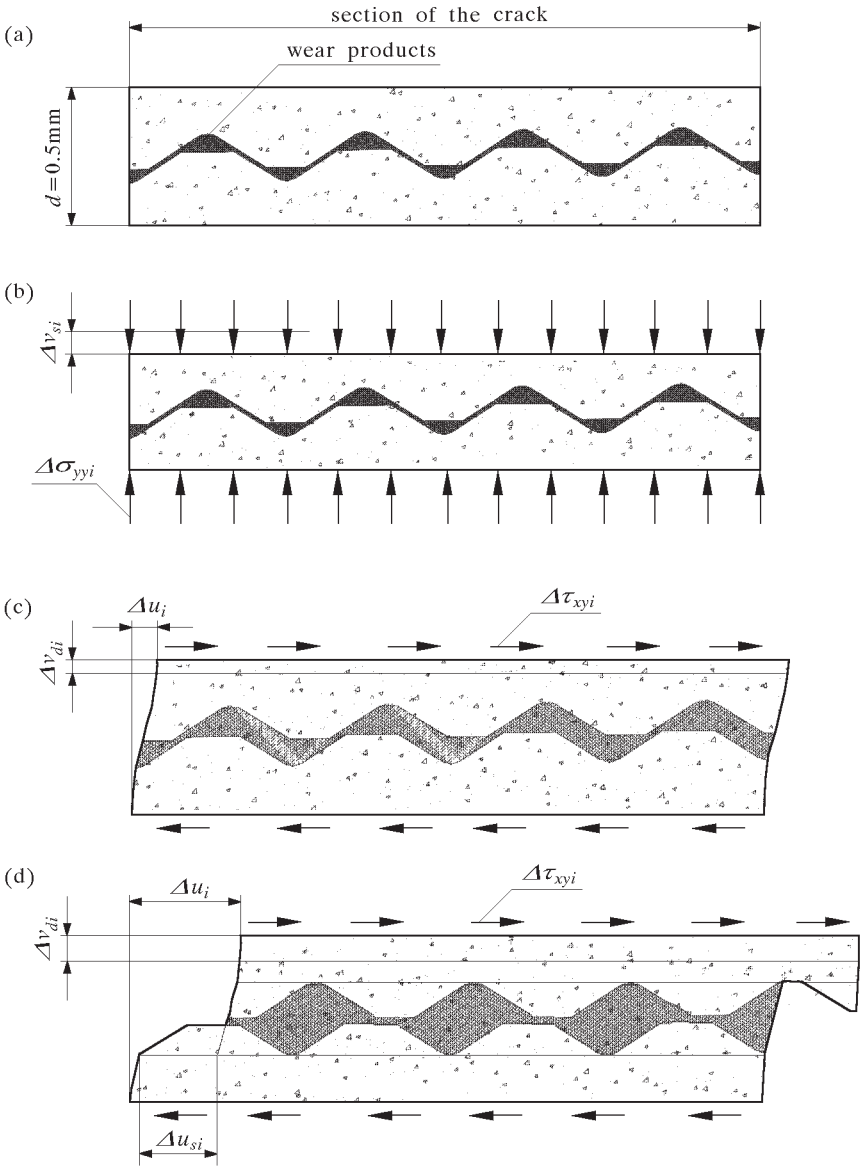

Fig. 16. Section of the specimen with the crack presented in a simplified form

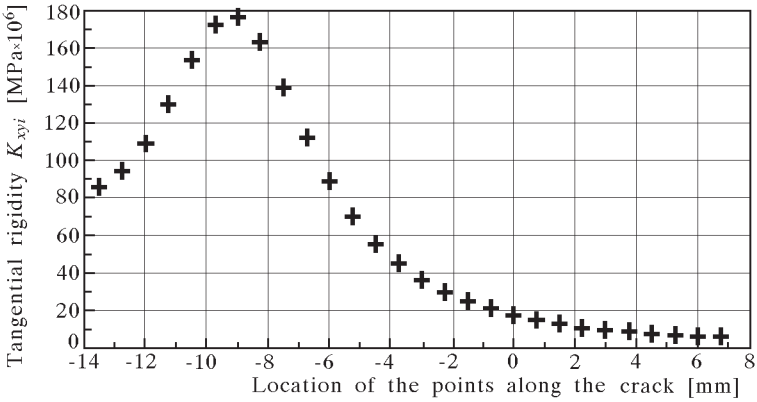

Fig. 17. Tangential rigidity K_{xyi} along the crack length at the third step of tangential load increasing at the constant normal load $P_n = 2600\,\mathrm{N}$

5. Numerical simulations of a crack propagation due to rolling contact loads

The analysis was focussed on seeking parameters, which affect most strongly values and amplitudes of the stress intensity factors (SIFs) at the crack tip during the wheel rolling process. In a 3D case the numerical simulation of a semi-elliptical squat type of crack observed in rail heads was performed taking into account the real shapes of wheel and rail, and interactions between the rail and wheel as well as crack faces due to a moving load.

The development of 3D analysis made before consisted in the works done in 1996-98 and aimed at finding of the effects of various parameters of contact. The crack size, normal and traction loads, residual stresses as well as stresses due to bending of the rail and rail temperature variation were investigated. The final results were presented in the Final Report RP 19 (Bogdański et al., 1995-96), while some selected results were published in Bogdański et al. (1998).

The squat was modelled as a plane oblique semi-elliptical crack at two stages of its development called "small" and "large" squats, respectively (Fig. 18).

In both cases, the cracks made an angle of 45° with the plane of rail symmetry, the semi-minor axis made an angle of 20° with the horizontal plane. The ratios between the semi-minor and semi-major axes of an ellipse were equal to 0.615 and 0.800 for the small and large squats, respectively. The profiles of the rail and a wheel are given in Fig. 18. The elliptical crack front was divided into 12 sections for the large squat and into 16 for the small one, respectively. All these sections were surrounded by eight special elements. The

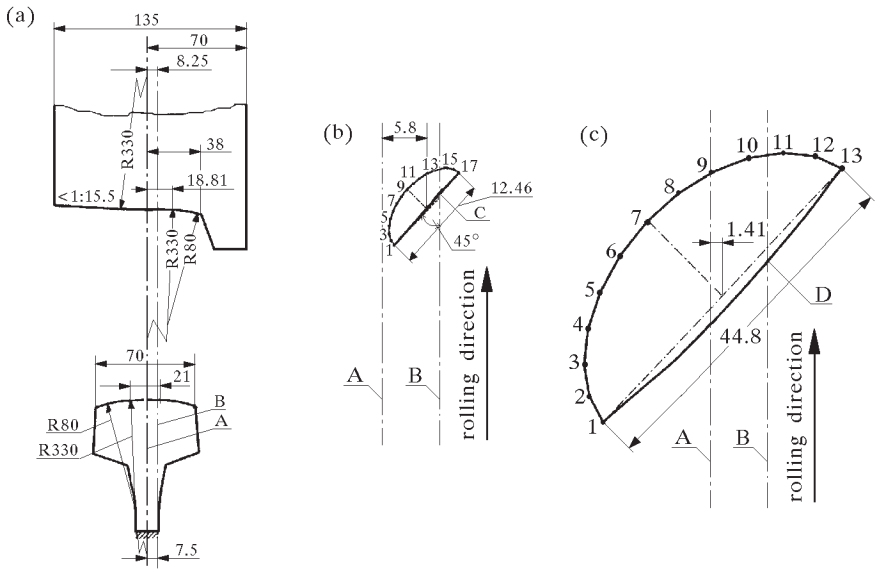

Fig. 18. Geometrical configuration of the system; A – rail axis; B – plane of rolling circle; C and D – reference points for the small and large squats, respectively; (a) profiles of rail and wheel adopted in analysis; (b) plan view of the small squat; (c) plan view of the large squat (all dimensions in mm)

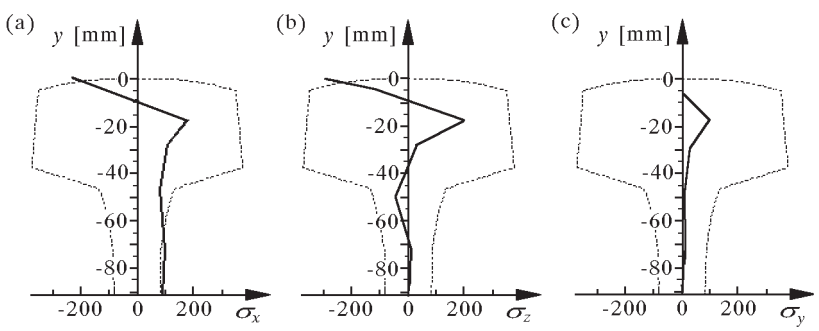

Fig. 19. Distributions of the residual stresses in the rail head; (a) longitudinal stress; (b) lateral stress; (c) vertical stress

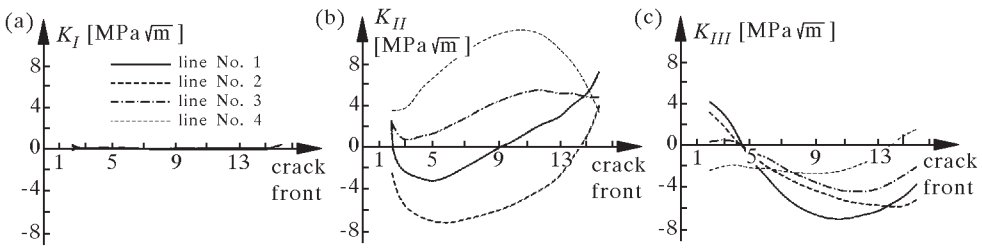

Fig. 20. Distributions of SIFs along the crack front: (a) K_I, (b) K_{II}, (c) K_{III}, for the wheel located at a distance of $x/b = -0.379$ ($x = -2.0$ mm) in four cases: line No. 1 – general case, line No. 2 – simplified case I with friction, line No. 3 – simplified frictionless case I, line No. 4 – simplified frictionless case II (for the description of the cases see Table 2)

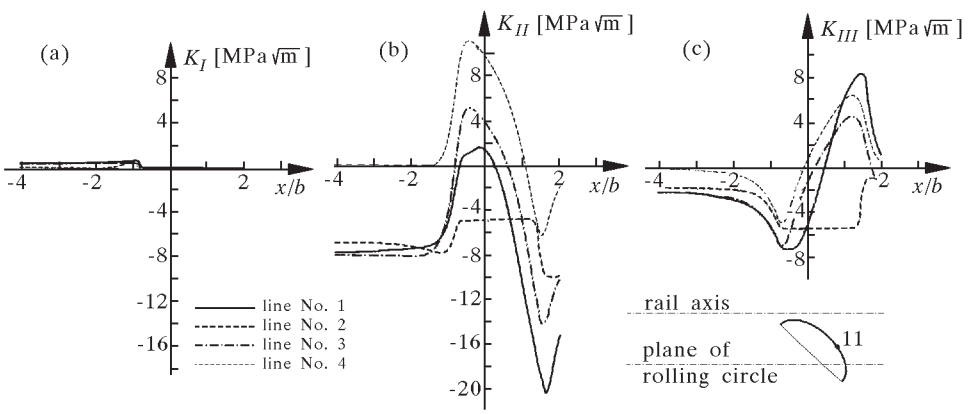

Fig. 21. The SIF courses: (a) K_I, (b) K_{II}, (c) K_{III}, at point No. 11 of the small squat front versus the position of the wheel, in four cases; line No. 1 – general case, line No. 2 – simplified case with friction I, line No. 3 – simplified frictionless case I, line No. 4 – simplified frictionless case II (for the point location see Fig. 18; for the description of the cases see Table 2)

wheel position in the course of rolling along the rail was determined relative to the reference points C and D shown in Fig. 18. The Coulomb friction between the crack faces as well as on the rail/wheel contact surface was assumed. The friction coefficient at the interfaces took different values. The distributions of components of the residual stresses over the rail head are given in Fig. 19.

The compressive stresses due to bending of the rail of the magnitude $\sigma_x = -83.5\,\mathrm{MPa}$ at the raceway surface of the rail and the uniform tensile thermal stress of the magnitude of $\sigma_x = 80.8\,\mathrm{MPa}$ produced by the temperature drop of $\Delta T = 35°\mathrm{C}$ were introduced into the considered cases.

Some selected results of investigations are given in Fig. 20, 21 and 22.

The diagrams of Stress Intensity Factors along the crack front at the load position $x/b = -0.379$ are shown in Fig. 20 (b is a half-width of the rail/wheel contact area, the parameters for each line are given in Table 2).

Table 2. Loading conditions applied to the considered two types of squat

Case	Size	R [kN]	T_x [kN]	σ_r [Mpa]	μ_{cr}	μ_s
General (Figs 20, 21, line No. 1)	small	130.0	28.0	$\sigma_x, \sigma_y, \sigma_z$ acc. to Fig. 19	0.1	0.4
Simplified with friction I (Figs 20, 21, line No. 2)	small	130.0	0.0	$\sigma_x, \sigma_y, \sigma_z$ acc. to Fig. 19	0.4	0.4
Simplified with friction I (Figs 20, 21, line No. 3)	small	130.0	0.0	$\sigma_x, \sigma_y, \sigma_z$ acc. to Fig. 19	0.0	0.0
Simplified with friction II (Figs 20-22, line No. 4)	small	130.0	0.0	no residual stress	0.0	0.0
Simplified with friction II (Fig. 22, line No. 5)	small	130.0	0.0	no residual stress	0.4	0.4
Simplified with friction III (Fig. 22, line No. 6)	large	130.0	0.0	no residual stress	0.0	0.0
Simplified with friction III (Figs 20-22, line No. 4)	large	130.0	0.0	no residual stress	0.4	0.4

The diagrams of Stress Intensity Factors versus the load position in the cases with and without friction, respectively, are given in Fig. 21.

Fig. 22 shows the diagrams of Stress Intensity Factors versus the load position for the small and large squats.

Concluding it can be stated that many factors contribute for the state of stresses at a tip of the crack and affect the Stress Intensity Factors. But the most significant and most uncertain ones are the interactions between the crack faces, which manifest through the value of friction coefficient between the crack faces. Further numerical models aim at finding a more accurate description of the process of crack faces interaction.

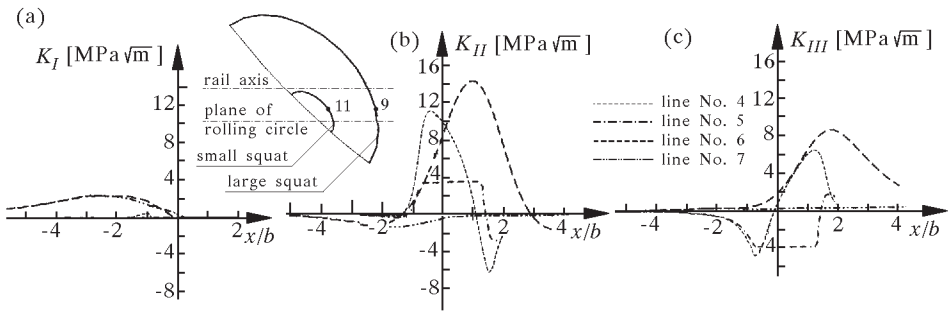

Fig. 22. Comparison between the SIF courses: (a) K_I, (b) K_{II}, (c) K_{III}, at the corresponding points No. 11 and 9 of small and large squats fronts. Line No. 4 – simplified frictionless case II for the small squat, line No. 5 -simplified case with friction II for the small squat, line No. 6 – simplified frictionless case III for the large squat, line No. 7 – simplified case III with friction for the large squat (for the point locations see Fig. 18; for the description of the cases see Table 2)

To include a wider variety of cases into consideration, further investigations were conducted using simpler 2D models, in which different ways of representation of the fatigue crack interaction were examined in detail (Olzak and Stupnicki, 1999a,b). To the 2D model of the rolling process of a cylinder along a raceway with a crack, shown in Fig. 23, the conditions of crack faces interaction presented in Fig. 24 were introduced.

From a variety of crack faces interaction models shown in Fig. 24 we will discuss two cases with the conditions of crack faces interaction adopted in Olzak and Stupnicki (2001):

- Crack faces covered with layers of a worn out material, the properties of which were determined basing on the results of experiments
- Crack faces covered with microaspherities, which force the experimentaly observed crack dilatation accompanying the tangential displacements.

5.1. The model with layers of a material of deteriorated properties covering the crack faces

It was assumed that the crack faces were covered with layers of the thickness $h = 100$ μm of a material of deteriorated properties with the characteristic parameters E^* and G^*. The values of these parameters accepted in calculations, i.e., $E^* = 0.2E$, $G^* = 0.025G$ resulted from the approximation of experimental results. The coefficient of friction between the crack faces co-

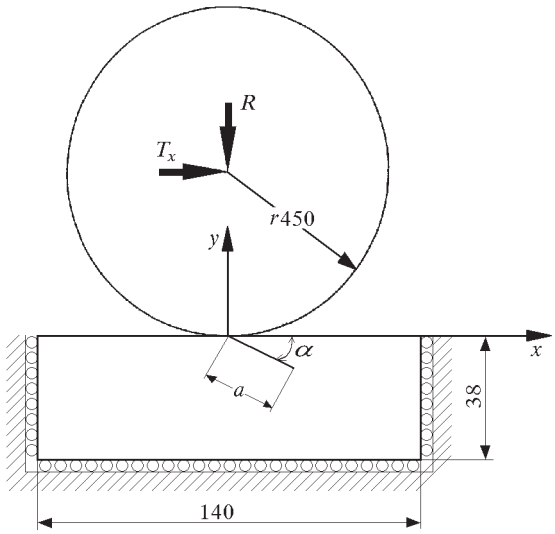

Fig. 23. 2D model under consideration

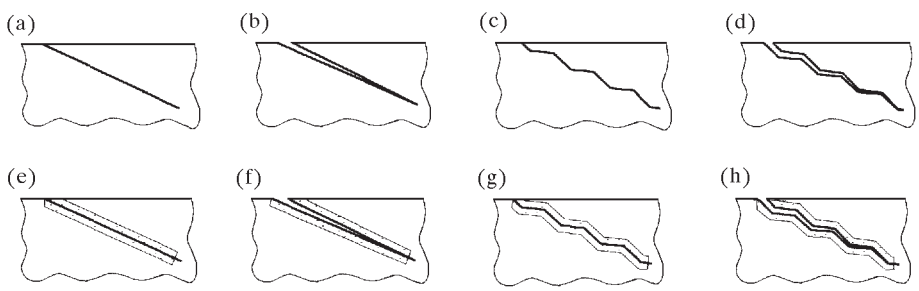

Fig. 24. Conditions of the crack faces interaction. The surface braking crack with the faces: (a) flat, (b) flat with a gap between them, (c) with a saw-like tortuosity, (d) with a saw-like tortuosity and a gap between them, (e) flat with layers of a material of deteriorated properties, (f) flat with layers of a material of deteriorated properties, and a gap between them, (g) with a saw-like tortuosity and with layers of a material of deteriorated properties, (h) with a saw-like tortuosity, layers of a material of deteriorated properties and with a gap between them

vered with wear deposits took the value $\mu_s = 1$ that corresponded to a high friction force appearing on a rough surface.

When such a big value of the coefficient of friction was assumed on the crack faces in the model with no layers of a material of deteriorated properties, the mutual displacements of crack faces were effectively reduced, blocking therefore the crack propagation according to Model II.

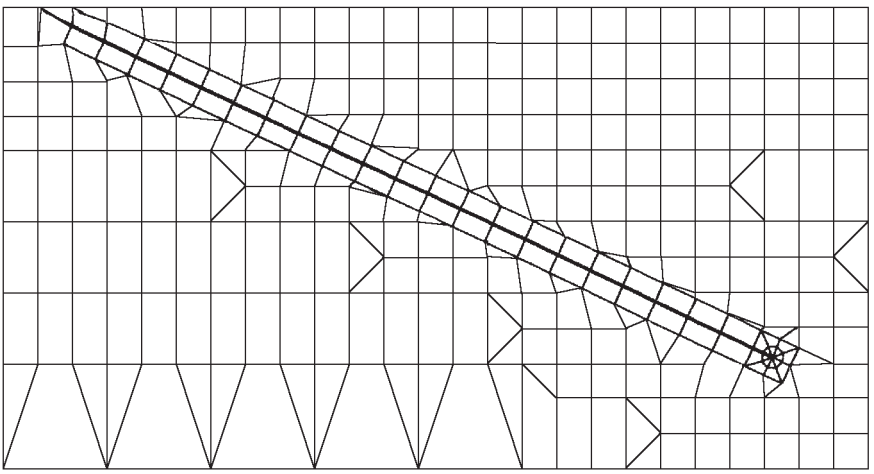

Fig. 25. Finite Element Mesh of the contact zone in the vicinity of crack

The FEM mesh of the contact zone in the vicinity of crack is shown in Fig. 25. Near the crack tip special elements have been employed, allowing for representation of singularities of the type $r^{-1/2}$. For solving the problem of contact with the friction included the whole process have to be analysed starting with the initial state far from the crack. After rolling a cylinder along a certain distance a stationary distribution of normal and tangential components of the forces between a cylinder and a raceway can be achieved. Then, the cylinder comes closer to the crack, which stimulates new forces on the contact surface as well as a new state of crack faces interaction. The algorithm for solution to this problem was given in Olzak et al. (1993). In the present investigations the calculations started at a distance of $x = 3b$, where b stands for half the contact length.

An essential influence of the crack on the pressure distribution over the contact surface has been detected within the range $-b < x < b$. Figure 26 shows the pressure distribution between the cylinder and raceway for several cylinder positions. The vicinity of crack affects the pressure peaks along the raceway at the crack mouths as well as the pressure redistribution when the

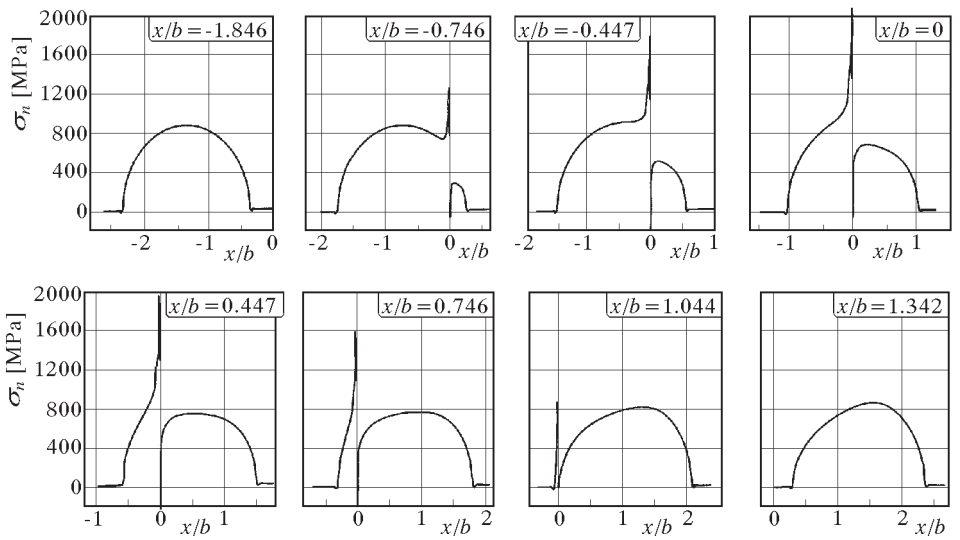

Fig. 26. Pressure distribution between the cylinder and raceway for several cylinder positions

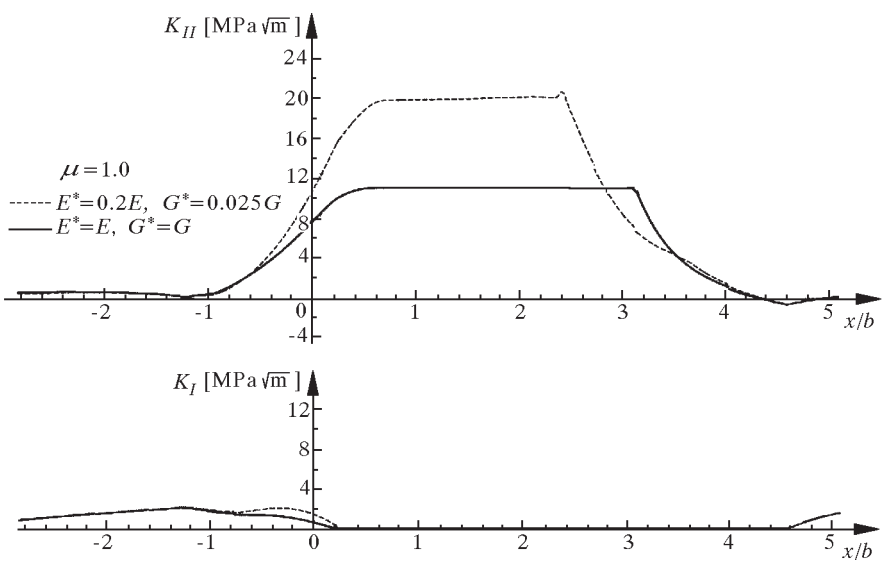

Fig. 27. Histories of SIF K_{II} versus the cylinder position

cylinder is rolling above the cracks. The dynamic load effects produced by the crack presence as functions of wheel velocity were discussed in paper Olzak and Szolc [26].

According to the Williams equation, the values of SIFs K_I and K_{II} were determined basing on the values of displacement vector components around the crack tip, which resulted from solving the contact problem. Figure 27 presents the histories of SIFs K_I and K_{II} in the case when the crack faces were covered with layers of worn out material, the properties of which were represented by the coefficients E^* and G^*. For comparison purposes the figure shows also the diagram representing the case when the layer of deposits was not considered with other conditions remaining the same. The diagram proves that two times higher values of ΔK_{II} amplitude were obtained in the case when the layers of material of deteriorated properties were introduced into the model.

5.2. The model of crack faces with apspherities forcing the crack dilatation

Basing on experimental observations of mutual displacements of the crack faces it can be stated that the tangential displacements Δu_s are accompanied by the displacements Δv_d, which act opposite to the compressive stresses pressing the crack faces against each other and represent the forced crack dilatation. In numerical simulation the simplified aspherities of the crack faces characterised by the slope angle γ, and not represented by the FEM mesh were adopted. That means that each displacement in the tangential direction δ_x is accompanied by the normal displacement of the magnitude $\delta_y = \delta_x \tan\gamma$ (Fig. 28).

Figure 29 shows the results obtained for the same loads as in the previous case for three different conditions of crack faces interaction. The following conditions were assumed: flat crack faces with the coefficient of friction $\mu = 0.4$ (line 1); crack faces covered with aspherities of the slope $\gamma = 25^\circ$, with an isotropic material surrounding the crack (line 2); crack faces covered with the same aspherities and, additionally, with layers of a material of deteriorated properties (line 3).

From the results of numerical simulations it is seen that the presence of aspherities reduces the value of $K_{II\,max}$ to 1/3 of its value in the case with no aspherities (cf lines 2 and 1), which is caused by preventing from microslips. However, when including the layers of worn out material together with the apherities one obtains the value of $K_{II\,max}$ two times higher (cf lines 3 and 2). Despite the fact that the value of $K_{II\,max}$ in the case of crack faces covered

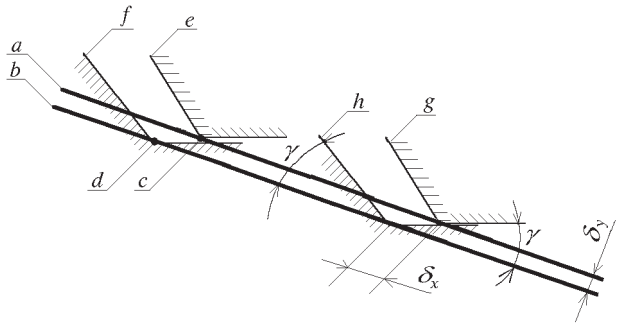

Fig. 28. Scheme of the crack covered with aspherities resulting from numerical simulations; a, b – upper and lower faces, respectively, of the crack represented by the FEM mesh; c, d – the pair of nodes in contact located on the opposite surfaces; f, h – modelled surfaces of roughness associated with nodes of the lower surface; e, g – modelled surfaces of roughness associated with nodes of the upper surface

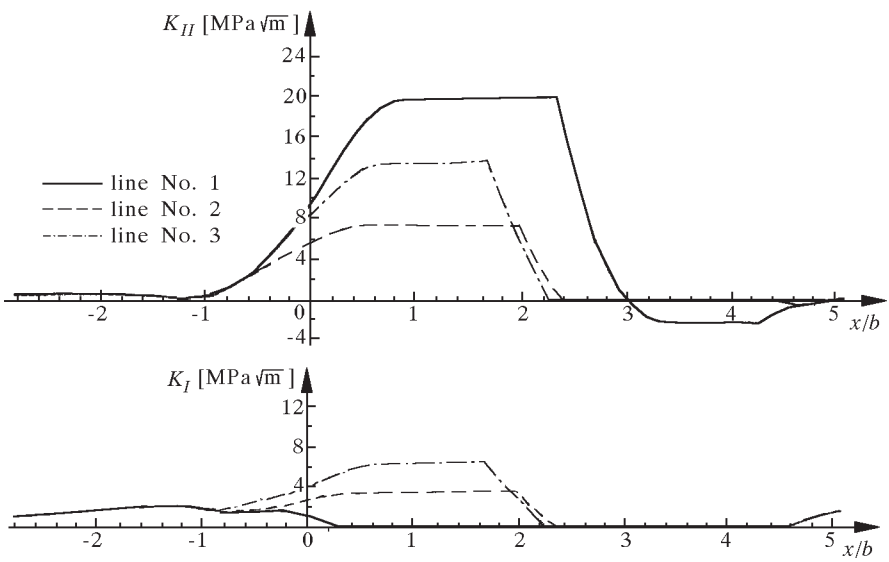

Fig. 29. Histories of the SIFs K_I and K_{II} versus the cylinder position

with asperities takes only 2/3 of its value in the case with flat faces, it should be noted that in this case, due to the crack dilatation, the SIF K_I appears.

6. Conclusions

The contact problems still raise intriguing questions with the local problems of contact becoming now most important in both the cognitive and practical aspects.

From the research discussed above the following conclusions can be drawn:

- The immersion method of Holographic Interferometry as well as Grating Holographic Interferometry, when employed in measurements of shapes of crack faces allow the reliable results to be obtained.
- The displacement vector components u and v were obtained at distances as small as $t \approx 0.25\,\text{mm}$ from the crack edges with the accuracy of $\delta u \approx \delta v \approx \pm 0.1\,\mu\text{m}$.
- The GHI method allows for observation of the processes of crack opening or closing, crack faces microslips as well as crack dilatation in the courses of load increasing and decreasing, respectively.
- A continuous distribution of the displacement vector components in the vicinity of crack enables determination of stress tensor components and deformation of the layer containing the crack. These values served as input data for the determination of normal and tangential rigidities of the layer containing the crack.
- The numerical simulations of bodies in contact with the squat type of crack have proved that substantial differences may arise between the results obtained depending on the model of crack faces interaction adopted.
- Introducing to the model the layers of material of deteriorated properties which cover the crack faces involves two times higher amplitudes of SIF K_{II} as compared to the case with no such layers introduced. This substantial difference brings about the SIF values which may affect the crack propagation despite taking the value of the coefficient of friction $\mu = 1$.

- The assumed values of E^*, G^* and h, remaining unchanged along the whole crack length were determined by means of averaging of the experimental results. The observations and measurements, however, show that these values vary along the crack length being also functions of load. Very small mutual displacements of the crack faces and no signs of surface wear affect very specific conditions in the vicinity of the crack tip. Along the central segment of the crack the wear signs are clearly visible, accompanied by the mutual displacements of crack faces, the magnitudes of which are close to the mean wavelength of roughness. In the vicinity of crack initiation a non-linear growth of wear was observed as well as mutual displacements of the crack faces exceeding the mean wavelength of roughness.

- The numerical simulations show that the presence of aspherities on the crack surfaces change substantially the phenomenon. Representing accurately the crack dilatation process they reduce the value of SIF $K_{II\,max}$ affecting, however, the appearance of SIF K_I.

- In further numerical investigations variable contact conditions along the crack length should be taken into account, as well as, if possible, their dependence on the load. The aspherities of crack surfaces should be also included.

References

1. *Aktualizacja katalogu wad szyn*, PKP, Centrum Naukowo-Techniczne Kolejnictwa, Warszawa, 1999

2. BATISTA A.C., DIAS A.M., LEBRUN J.L., LE FLOUR J.C, INGLEBERT G., 2000, Contact Fatigue of Automotive Gears: Evolution and Effects of Residual Stresses Introduced by Surface Treatments, *Fatigue Fract. Engng. Mater. Struct.*, **23**, 217-228

3. BIJAK-ŻOCHOWSKI M., MAREK P., 1997, Residual Stress in Some Elasto-Plastic Problems of Rolling Contact with Friction, *International Journal of Mechanical Sciences*, **39**, 1, 15-32

4. BOGDAŃSKI S., 1999, *Growth of the Rolling Contact Fatigue Cracks in the Presence of Liquid*, Publishing House of the Warsaw University of Technology, Warsaw (in Polish)

5. Bogdański S., Olzak M., Stupnicki J., 1995-96, *Stress Analysis of Rail Rolling Contact Fatigue Cracks*, The European Rail Research Institute, Utrecht, The Netherlands, Final Report, RP. 19

6. Bogdański S., Olzak M., Stupnicki J., 1996, Influence of Liquid Interaction on Propagation of Rail Rolling Contact Fatigue Cracks, *Proceedings of the 2nd Mini Conference on Contact Mechanics and Wear of Rail/Wheel Systems*, Budapest, 134-143

7. Bogdański S., Olzak M., Stupnicki J., 1996b, Numerical Stress Analysis of Rail Rolling Contact Fatigue Cracks, *Wear*, **191**, 14-24

8. Bogdański S., Olzak M., Stupnicki J., 1998, Numerical Modelling of a 3D Rail RCF "Squat"-Type Crack Under Operating Load, *Fatigue and Fracture of Engineering Materials and Structures*, 923-935

9. Bover A.F., 1988, The Influence of Crack Faces Friction and Trapped Fluid on Surface Initiated Fatigue Crack, *ASME Journal of Tribology*, **110**, 704-711

10. Deroche R.Y., Bettemborg J.P., Prasil B., Bertrand J.P., Juckum C., 1993, Rolling Contact Fatigue Cracks on S.N.C.F. Conventionnal Tracks, In: *Rail Quality and Maintenance for Modern Railway Operation*, Kluver Academic Publischer, Netherlands

11. Dubourg M.C., Kalker J.J., 1993, Crack Behaviour Under Rolling Contact Fatigue, In: *Rail Quality and Maintenance for Modern Railway Operation*, Kluver Academic Publischer, Netherlands

12. Gohar R., Cameron A., 1966, The Mapping of Elastohydrodynamic Contacts, *ASLE Preprints 66*, **LC 21**

13. Grubin A., 1949, *Osnovy gidrodinamicheskeĭ teorii smazki tyazhelo nagruzenykh cylindricheskikh powerkhnosti*, CNITMASZ KN.30

14. Hertz H., 1882, Über die Beruhnung fester elastischer Korper, *J. Reine Angewandte Mathematic*, **92.156**

15. Kannel J.W., 1965-66, Measurements of Pressure in Rolling Contact, *Proc. Inst. of Mech. Eng.*, **180**, Pt. 3B

16. Kannel J.W., Bell J., Allen C., 1965, Methods for Determining Pressure Distribution in Lubricated Rolling Contact, *ASLE*, **8**

17. *Katalog uszkodzeń i złamań szyn*, Wydawnictwa Komunikacyjne, Warszawa, 1959

18. Keer L.M., Briant M.D., 1983, A Pitting of Rolling Contact Fatigue, *Journal of Lubr. Techn., Trans. ASME*, **105**, 198-205

19. Krzemiński-Freda H., 1969, Rozkład ciśnienia i kształt filmu olejowego przy współpracy elementów tocznych smarowanych elastohydrodynamicznie, Rozprawa doktorska, Łódź

20. Lisegang R., 1969, Der nichtisoterme hydrodynamishe Schmiefilm zwishen hochbelasteten elastische Walzen, *VDI-Z.*, 1, **14**

21. Merritt H.M., 1935, Worm Gear Performance, *Proc. Inst. Mech. Eng.*, London, **129, 127**

22. Olzak M., Stupnicki J., 1999a, The Influence of Crack Faces Interaction Model on the Results of Numerical Study of Stress Intensity Factors for the Surface Breaking Cracks in Race Way, *Int. Conf. on Contact Mechanics'99*, Stuttgart

23. Olzak M., Stupnicki J., 1999b, Variations of the Stress Intensity Factors in the Process of Load Rolling Along a Race Conatining a Crack. Part I and II, *Proc. of VII Conference on Fracture Mechanics*, Kielce Cedzyna, 109-123 (in polish)

24. Olzak M., Stupnicki J., 2001, Numerical Study of the Stress Intensity Factors for Cracks in Raceways with the Experimentally Determined Interaction Between Crack Faces, *Conference on Contact Mechanics*, Sevilla, 18-20 June

25. Olzak M., Stupnicki J., Wójcik R., 1993, Numerical Analysis of 3D Cracks Propagating in the Rail-Wheel Contact Zone Rail Quality and Maitanance for Modern Railway Operationed, By J.J. Kalker, D.F. Cannon, O. Orringer, Kluver Academc Publishers, 385-395

26. Olzak M., Szolc T. Dynamics Effects Caused by "Squat" type Crack in Race Way of the Rails. To be published

27. Pepler W., 1938, Druckubertragung an geschmierte zylindrischen Glait und Walzflachen, *VDI – Forschunghefte*, **391**

28. Pyrzanowski P., 1997, Wpływ naprężeń własnych na rozwój pęknięć zmęczeniowych w strefie kontaktu, Rozprawa doktorska na Wydziale Mechanicznym Energetyki i Lotnictwa Politechniki Warszawskiej, Warszawa

29. Pyrzanowski P., Mruk I., 2000, Investigation of "Squat"-Type Crack Development in Heads of Rails, *Proceedings of 17th Danubia-Adria Symposium on Experimental Methods in Solid Mechanics*, Praga, Czech Republic, October

30. Pyrzanowski P., Stupnicki J., 2001, Evaluation of Contact Rigidity of Fatigue Crack Faces for Numerical Models of RCF Crack Growth, *GESA Symposium*, Chemnitz, 17-18 May

31. Stupnicki J., 1971, Photoelastic Study of Influence of Oil Film on Contact Stresses, *Int. J. Mech. Sci.*, Pergamon Press, **13**

32. Szpakowska M., 2000, Determination of Rigidity of a Layer Conating a Fatigue Crack under Normal and Tangential Loads Acting Simultaneously, PhD Thesis, Warsaw University of Technology, Warsaw (in Polish)

33. Świderski Z., 1992, Naprężenia własne szyn kolejowych, *Materiały XV Sympozjum Mechaniki Eksperymentalnej Ciała Stałego*, Jachranka, 270-278

Problemy mechaniki kontaktu – rozwój pęknięć zmęczeniowych w warstwie wierzchniej

Streszczenie

Praca dotyczy rozwoju pęknięć zmęczeniowych w warstwie wierzchniej, obecnie jednego z najbardziej aktualnych problemów mechaniki kontaktu. Przedstawia uzyskane przez autorów wyniki eksperymentalnych i numerycznych poszukiwań czynników, które mogą mieć istotny wpływ na rozwój pęknięć zmęczeniowych typu "squat" dla kontaktu koła i szyny.

W pierwszej części pracy przedstawiono wyniki obserwacji i pomiarów metodą immersyjną interferometrii holograficznej powierzchni rzeczywistych pęknięć wykrytych w główkach szyn kolejowych oraz wyniki uzyskane metodą siatkową interferometrii holograficznej, badania wzajemnego oddziaływania brzegów pęknięć w próbkach ze stali 900A podczas działania złożonych stanów obciążenia.

W drugiej części pracy przedstawiono wyniki badań numerycznych przypadków 3D pęknięć typu "squat", uwzględniających złożone stany obciążenia kontaktu, naprężenia od zginania szyny, naprężenia własne i naprężenia wynikłe ze zmiany temperatur. Przedstawiono także dla obiektów 2D badania wpływu warunków oddziaływania brzegów pęknięcia na wyniki symulacji. Rozważono osiem różnych przypadków, prezentując wyniki w postaci wykresów współczynnika intensywności naprężenia K_{II} w funkcji położenia obciążenia względem pęknięcia.

W ostatniej części przedstawiono wyniki symulacji przetaczania walca po bieżni ze skośnym pęknięciem, którego warunki oddziaływania brzegów wyznaczono na podstawie badań eksperymentalnych.

Manuscript received March 21, 2001; accepted for print April 20, 2001